2D Materials

PAPER

RECEIVED
12 September 2018

REVISED
22 October 2018

ACCEPTED FOR PUBLICATION
6 November 2018

PUBLISHED
22 November 2018

Quasiparticle electronic structure of honeycomb C_3N: from monolayer to bulk

Yabei Wu[1,2,3], Weiyi Xia[2,3], Weiwei Gao[2], Fanhao Jia[1], Peihong Zhang[1,2] and Wei Ren[1]

[1] Department of Physics, International Centre for Quantum and Molecular Structures, Materials Genome Institute, Shanghai University, 99 Shangda Road, Shanghai 200444, People's Republic of China
[2] Department of Physics, University at Buffalo, State University of New York, Buffalo, NY 14260, United States of America
[3] YW and WX contributed equally to this work.

E-mail: pzhang3@buffalo.edu **and** renwei@shu.edu.cn

Keywords: electronic structure, density functional theory, quasiparticle calculation, 2D C_3N

Abstract

Layer-dependent quasiparticle band structures of the newly emerged honeycomb C_3N are systematically studied using both density functional theory and GW methods. The calculated GW band gap for monolayer C_3N is about 1.5 eV. This moderate band gap may be ideal for future electronics applications. Our result is in marked contrast with a recent experimental report of 0.39 eV and calls for future experimental verifications. Interlayer chemical coupling effects on the electronic structure of C_3N are investigated using several bilayer models. The electronic structure of bilayer C_3N depends sensitively on the layer stacking pattern with the calculated quasiparticle band gap ranging from 0.87 to 1.35 eV. Finally, we illustrate the effects of interlayer chemical interaction and bulk dielectric screening on the electronic properties of C_3N. Depending on the specific bulk stacking, C_3N may be metallic or semiconducting with a narrow gap of about 0.6 eV, even though different bulk phases are essentially degenerate energetically. As a result, it may be challenging to prepare single-phase semiconducting bulk C_3N unless synthetic kinetics can somehow prefer or prohibit certain stacking patterns. This issue deserves further investigations.

Introduction

The intrinsic zero band gap of graphene severely limits its potential applications in semiconductor devices, and tremendous efforts have been made to induce a finite band gap in graphene through graphene-substrate interactions [1–4] or chemical doping [5, 6]. Unfortunately, weak interfacial interactions typically produce a band gap that is too small for electronics applications whereas chemical doping tends to introduce significant structural and electronic distortions, rendering graphene to lose most of its defining properties and advantages. Therefore, there is significant current interest in the search for two dimensional (2D) semiconductors for electronics applications, and the discovery of graphene-like ordered carbon–nitrogen systems, including C_3N_4 [7, 8], C_4N_3 [9], C_5N [10], and, in particular, C_3N has generated much recent research excitement.

Highly ordered honeycomb structure carbon nitrogen alloy C_3N was first proposed theoretically [11] using the particle-swarm optimization method [12] combined with a cluster-expansion technique and has recently been successfully synthesized [13, 14]. This structure was later confirmed as the most energetically favorable among all possible 25% nitrogen doping configurations [15]. The predicted (indirect) band gap for monolayer C_3N was about 0.3 eV, which was calculated using the local density approximation (LDA) to the exchange correlation functional in density function theory (DFT). This result would suggest that the true quasiparticle gap of monolayer C_3N be in the desirable range for electronics applications considering that the DFT-LDA or the DFT-GGA (generalized gradient approximation) approach almost always underestimates the band gap of semiconductors. In fact, one expects a greater quasiparticle self-energy correction for 2D systems than that for their 3D counterpart due to the weak dielectric screening in 2D systems. Surprisingly, the measured band gap of the C_3N quantum dots (QD) as a function of the lateral sample size converges to about 0.39 eV [13] at large sizes, which agrees remarkably well with the DFT-LDA result [11] for monolayer C_3N.

It is highly unlikely that DFT-LDA/GGA calculations can *accidently* predict the correct quasiparticle band gap for C_3N and other 2D semiconductors. For example, the DFT band gap for free-standing monolayer black phosphorus is about 0.89 eV, to be compared with the quasiparticle band gap of 2.08 eV and the optical gap of 1.6 eV [16]. Therefore, the claimed agreement between DFT and experimental results for C_3N is rather intriguing and deserves scrutiny. It is not clear if the experimental measurements were done on free-standing monolayer C_3N or not. Quasiparticle properties of isolated monolayer systems are fundamentally different from those of monolayer on substrates. In addition, excitonic effects may also play a role in the experiment. Regardless, comparing experimental values with the DFT result for monolayer is not justified.

In this work, we have carried out detailed DFT and GW [17, 18] quasiparticle calculations for monolayer, bilayer, and bulk C_3N, aiming at illustrating the layer-dependent dielectric screening effects and the inter-layer chemical interaction on the quasiparticle properties. We find that the fully converged GW band gap for monolayer C_3N is about 1.5 eV, in stark contrast with the claimed experimental result of about 0.39 eV [13]. Therefore, we conclude that the experimental results [13] should not be compared with those for monolayer C_3N. Understanding the quasiparticle properties of bilayer and bulk phases of C_3N is more challenging. The stacking patterns here are much more complicated than those of graphene layers. We find that several possible layer stacking patterns are essentially degenerate within the theoretical accuracy, with the exception of the simple AA stacking which is noticeably higher in energy. The calculated energy differences between several different stacking patterns are also much smaller than the thermal energy at room temperature. It is likely that no single stacking pattern may dominate in the as-synthesized samples. We find that the quasiparticle band structure, in particular, the quasiparticle band gap, is very sensitive to the stacking pattern, both for the bilayer and bulk phases. Interlayer chemical coupling reduces the calculated quasiparticle band gap of bilayer systems to 0.87–1.35 eV. Depending on the assumed stacking pattern, the bulk phase could be a narrow gap semiconductor with a band gap of about 0.6 eV or could be a metal. Our results call for future experimental clarifications.

Computational details

All structures are optimized with pseudopotential plane wave based DFT methods as implemented in the vienna *ab initio* simulation package (VASP) [19, 20]. The GGA functional of Perdew–Burke–Ernzerhof (PBE) [21] and two van der Waals (vdW) functionals, optB86b-vdW [22] and SCAN+rVV10 [23], are used in this work for structural optimizations. Including the vdW interaction in the structural optimization is important for these layered materials since their electronic properties can be sensitive to the interlayer spacing/interactions. The structures are fully optimized until the energy difference between two successive steps is smaller than 10^{-5} eV and the forces on the atoms are less than 10^{-3} eV Å^{-1}. For the Brillouin zone sampling, we used a $9 \times 9 \times 1$ Monkhorst–Pack [24] k-grid for monolayer and bilayer C_3N and a $9 \times 9 \times 6$ k-grid for bulk C_3N. In the DFT calculations for the monolayer and bilayer C_3N, a vacuum space of at least 15 Å thick is included in the supercell to minimize the fictitious interactions between neighboring layers.

The quasiparticle band structures are calculated within the GW approximation [17] using a local version of the BERKELEYGW package [18] in which the recently developed acceleration method [25] is implemented. Our new method [25] significantly accelerates fully converged GW calculations without sacrificing the accuracy. Briefly, this method takes advantage of the analytical behavior of the density of states (DOS) of materials at high energies and approximates the summation over high-energy unoccupied bands in the dielectric function and self-energy calculations with an integration over an energy grid. The Hybertsen–Louie generalized plasmon-pole model (HL-GPP) [17] is used to extend the static dielectric function to finite frequencies. In GW calculations for monolayer and bilayer systems, a truncated Coulomb potential [26] is used to accelerate the convergence of the calculated results with respect to the interlayer separations. Other details of the GW calculations will be discussed later.

Results and discussion

Monolayer C_3N

We first discuss the electronic structure of monolayer C_3N to illustrate the importance of the self-energy correction and the convergence behavior of the GW results for 2D materials. Figure 1(a) shows the crystal structure of monolayer C_3N, which can be considered as a 2×2 graphene supercell with 25% nitrogen substitutions. This highly ordered carbon–nitrogen alloy structure has been shown to be the most stable structure among all of the possible 25% nitrogen doping configurations [15]. The DFT-PBE and GW band structures are shown in figure 1(b). The calculated DFT-PBE minimum indirect band gap is 0.39 eV, with the valence band maximum (VBM) located at the M point and the conduction band minimum (CBM) located at the Γ point. Our DFT result agrees well with previous work [27, 28]. The fully converged GW results give an indirect band gap (M to Γ) of about 1.50 eV as shown in figure 1(b), which is over 1.1 eV larger than the DFT-PBE result and 0.54 eV larger than that calculated using the HSE06 hybrid functional [11].

As we have mentioned earlier, it was reported that the measured band gap of (monolayer) C_3N QD conv-

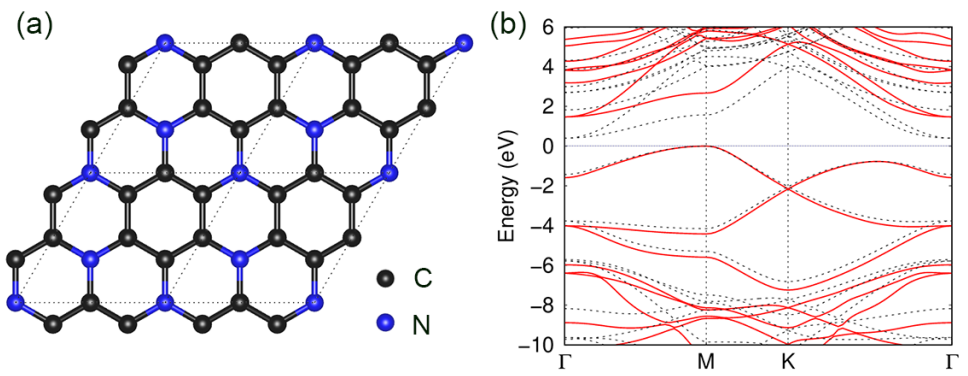

Figure 1. (a) Crystal structure of monolayer C_3N. (b) Band structures of monolayer C_3N calculated within the DFT-PBE method (black dotted lines) and the GW method (red solid lines).

erges to 0.39 eV as the lateral size of the QD increases. This value agrees surprisingly well with the calculated DFT band gap of monolayer C_3N. Our GW results clearly indicate that the measured band gap [13] cannot be interpreted as that for (isolated) monolayer C_3N and that the comparison between the experiment and the DFT results for monolayer C_3N is not justified. Several factors may contribute to this *accidental* agreement, among which interfacial chemical interaction and screening effects from the substrate (or from multilayer C_3N) are the most plausible ones if serious experimental errors can be excluded.

The band gaps of 2D materials are often very sensitive to the substrate (or multilayer) screening effects. In addition, interfacial or interlayer chemical interactions can also substantially modify their fundamental gap. This is particularly true for C_3N since the band edge states are mostly derived from carbon p_z orbitals with small admixtures of nitrogen p_z as shown in figure 2. These out-of-plane oriented states are especially susceptive to interfacial and/or interlayer chemical interactions as we will discuss later.

We now discuss the convergence behavior of the GW results with respect to various numerical parameters. GW calculations are still relatively expensive even with today's powerful computers, and sometimes imposing numerical cutoffs is not just a convenience but a requirement. However, it is very important to ensure that the calculated results are adequately converged with respect to the numerical cutoffs since under-converged results may give rise to false predictions. For bulk solids, the two most important truncations are the kinetic energy cutoff for the dielectric matrix and the number of conduction states included in the GW calculations as we have discussed in detail in our previous work [25, 29–31]. GW calculations for 2D materials are met with additional challenges due to the extremely slow convergence of the GW results with respect to the density of the k-grid used in the Brillouin zone integration. These convergence issues must be carefully checked.

The upper panel of figure 3 shows the convergence behavior of the calculated minimum indirect (M to Γ) band gap of monolayer C_3N with respect to the number of conduction bands included in the GW self-energy summation and the kinetic energy cutoff of the dielectric matrix. The bottom panel of figure 3 shows similar convergence behavior for the direct band gap at the Γ point. We mention that all conduction bands are effectively included in the dielectric function calculations. The calculated minimum band gap varies from less than 1.25 eV (under-converged) to about 1.50 eV (fully converged). An enormous number (over 10 000) of conduction bands need to be included in the GW summation to achieve a converged result. In addition, a large cutoff energy of about 60 Ry for the dielectric matrix is required for this system. These computational challenges make accurate GW predictions for large and/or complex systems very difficult. Using our recently developed acceleration method [25], which greatly reduces the computational cost associated with the band summation in the GW calculations, we are able to achieve highly converged GW results for this system with about 800 conduction band (integration points), to be compared with the requirement of over 10 000 bands using the conventional band-by-band summation method.

Fully converged GW calculations for 2D materials pose additional challenges. In GW calculations, the Brillouin zone integration of the quasiparticle self-energy correction $\Sigma_{n\vec{k}}$ for state $|n\vec{k}>$ is often carried out on a uniform k-grid: $\Sigma_{n\vec{k}} = \sum_{\vec{q}} f_{\vec{q}} \sum_{n\vec{k}}(\vec{q})$. For bulk solids, this summation usually converges quickly with increasing k-grid density. For 2D materials, however, the convergence is extremely slow [31–34] due to the analytical behavior of the 2D dielectric function and other relevant quantities as q approaches 0. Recently, we have successfully developed a combined subspace sampling and analytical integration method that can drastically reduce the required k-grid density for achieving fully converged GW results for 2D materials. Our method is inspired by a recent work [31] in which the authors proposed a nonuniform sampling scheme in the GW calculations. Briefly, the above-mentioned Brillouin zone integration is carried out in two steps: $\sum_{n\vec{k}} = \sum_{\vec{q}\neq 0} f_{\vec{q}} \sum_{n\vec{k}}(\vec{q}) + \frac{f_0}{V_{mBZ}} \int_{mBZ} \Sigma_{n\vec{k}}(\vec{q}) d\vec{q}$.

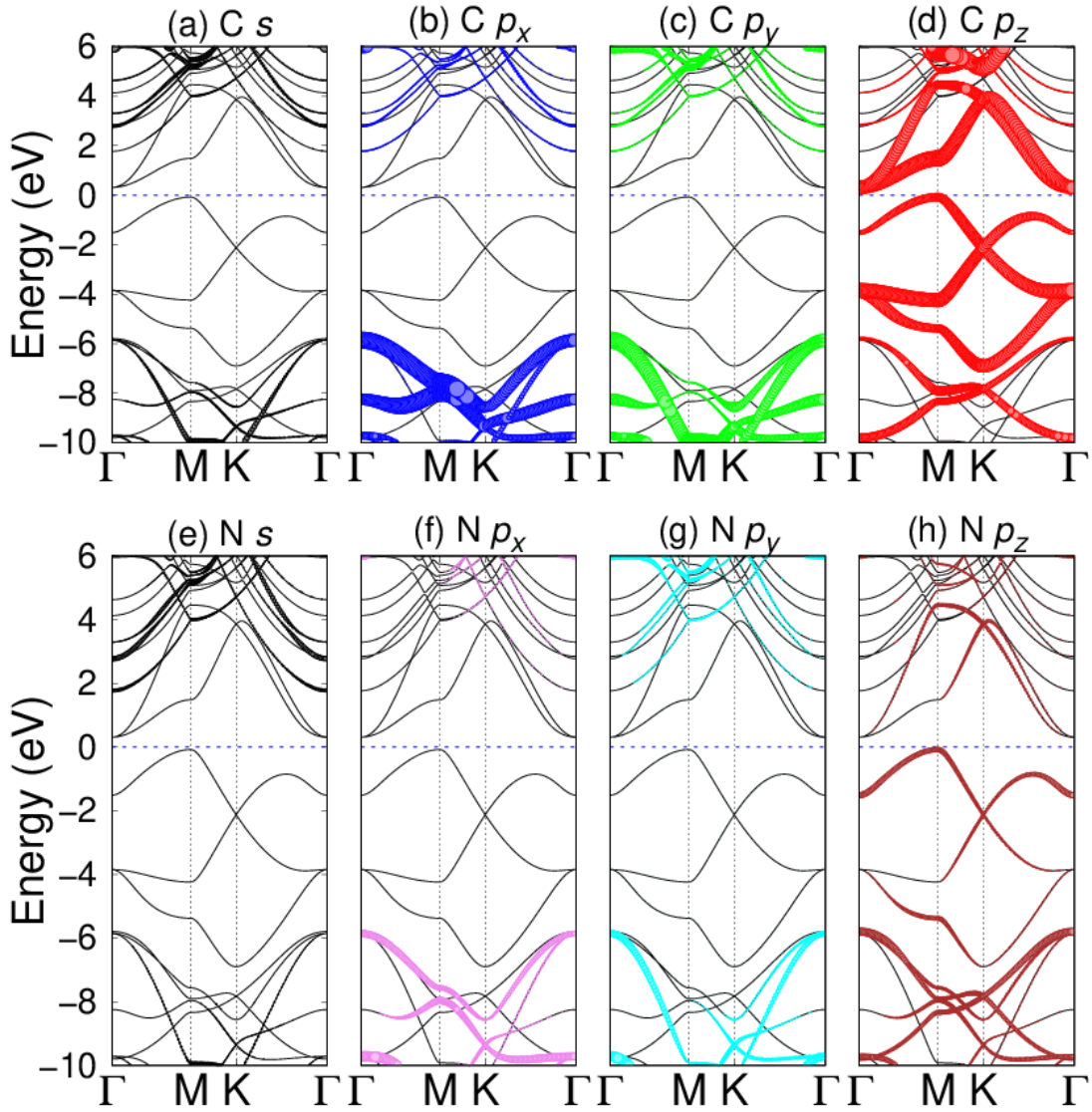

Figure 2. Decomposition of the Bloch wave functions into contributions from atomic orbitals. The band edge states are mostly derived from carbon p_z orbitals with small admixtures of nitrogen p_z.

The integration over the mini-Brillouin zone (mBZ) enclosing the Γ ($\vec{q} = 0$) point is treated separately: we first calculate the quantity $\Sigma_{n\vec{k}}(\vec{q})$ for several q points within the mBZ. The results are fit with some analytical function and the integration over the mBZ can then be calculated analytically. Figure 4 compares the performance of this new method with the conventional uniform sampling technique. Using this newly developed method, we are now able to achieve adequately converged GW results (to within 0.02 eV) using a $6 \times 6 \times 1$ k-grid. In contrast, using the conventional method, one would need an extremely dense k-grid of $24 \times 24 \times 1$ to achieve a similar level of convergence. We will report the detail of our method in a separate publication.

Bilayer C_3N

We now consider bilayer structures to illustrate the effects of the interlayer chemical interaction (hybridization). As we have discussed in the previous section, we expect that the band-edge states of C_3N be significantly affected by the interlayer chemical coupling since they are mostly derived from the out-of-plane p_z orbitals. To this end, we construct four bilayer C_3N structures with different stacking patterns as shown in figure 5. In the AA1 structure, all atoms in the top layer are located directly on top of the same atoms in the bottom layer. The AA2 stacking can be regarded as shifting the top layer in the AA1 stacking by half lattice constant along the diagonal direction. In the AA2 stacking, all atoms in the top layer are still directly above those in the bottom layer. However, the nitrogen-nitrogen pairs are avoided. The AB1 (AB2) stacking is obtained by taking the AA1 (AA2) structure and shifting the two layers along diagonal direction by 1/3 of the lattice constant.

Interlayer chemical interaction is very sensitive to the interlayer separation which can be more accurately calculated using vdW density functionals such as optB86b-vdW [22] or SCAN+rVV10 [23] compared with local or semilocal functionals. Table 1 shows the optimized crystal structures using three different

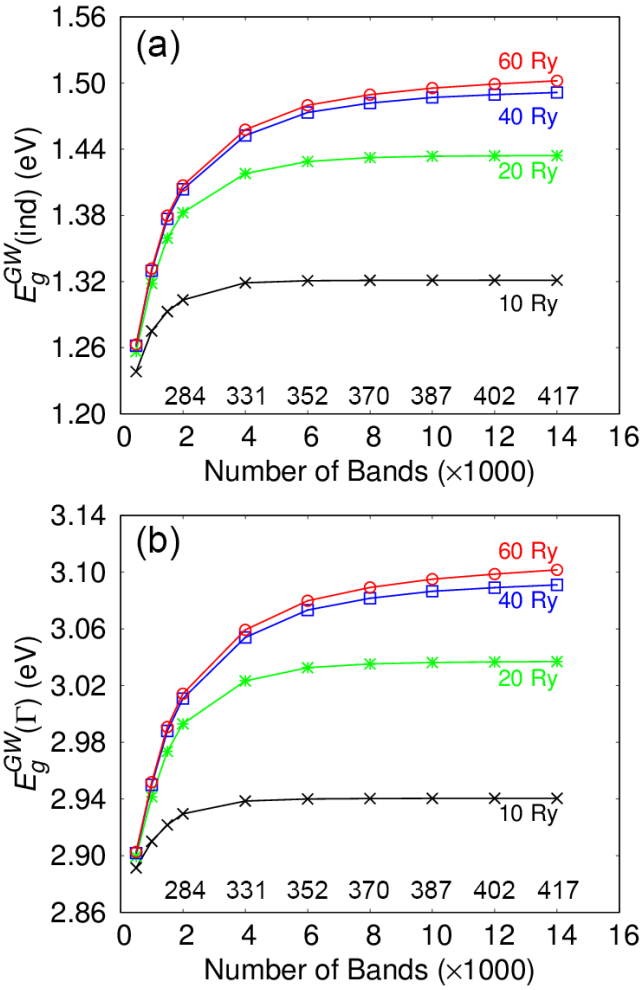

Figure 3. Convergence behavior of the calculated GW band gap for monolayer C_3N with respect to the number of conduction bands included in the self-energy summation and the cutoff for the dielectric matrix. (a) The minimal indirect gap; (b) the direct band gap at the Γ point.

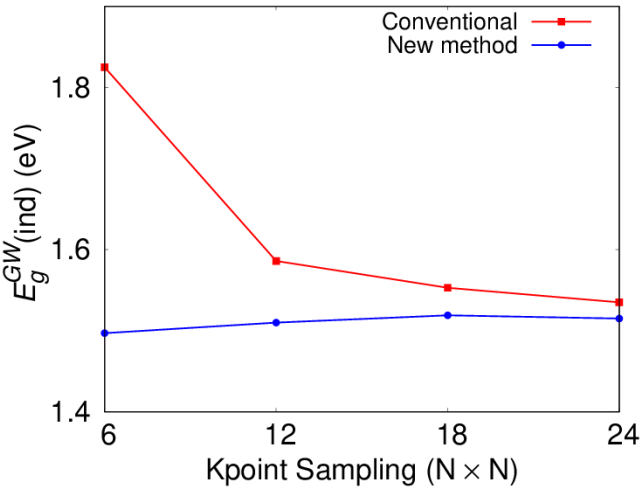

Figure 4. Calculated GW band gap of monolayer C_3N as a function of the in-plane *k*-point sampling density. The red curve shows the results calculated using the conventional uniform *k*-point sampling method, whereas the blue curve is from the new method described in the text.

energy functionals. Both vdW functionals predict an interlayer separation between 3.26 and 3.40 Å, whereas the PBE functional significantly overestimates this separation. Within the vdW DFT approaches, the AA1 structure is slightly higher (about 5 meV/atom) in energy, whereas the other three structures are essentially degenerate within theoretical accuracy with an energy difference of less than 1 meV/atom. With such a

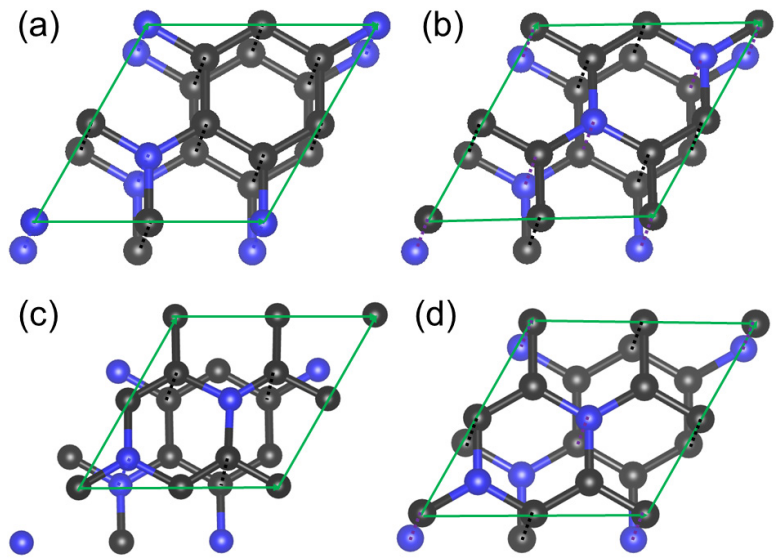

Figure 5. Four bilayer C_3N structures, namely (a) AA1, (b) AA2, (c) AB1, and (d) AB2.

Table 1. Optimized structural parameters for the four bilayer structures (a is the in-plane lattice constant and d is the interlayer distance) and their relative energies (meV/atom) using different functionals.

Functional	PBE			optB86b-vdW			SCAN +rVV10		
Stacking	a (Å)	d (Å)	Energy (meV)	a (Å)	d (Å)	Energy (meV)	a (Å)	d (Å)	Energy (meV)
AA1	4.861	4.198	0.4	4.859	3.385	5.5	4.830	3.401	5.6
AA2	4.861	4.104	0.0	4.859	3.268	0.4	4.831	3.289	0.8
AB1	4.861	3.942	0.4	4.859	3.262	0.9	3.830	3.283	0.7
AB2	4.860	4.048	0.0	4.859	3.265	0.0	4.830	3.268	0.0

small energy difference, it is likely that no single stacking will dominate at room temperature.

For simplicity, we will use only the structures optimized with the optB86b-vdW functional for both DFT and GW electronic structure calculations. Figure 6 shows the DFT-PBE band structures of four bilayer C_3N systems. The calculated DFT band gap varies from 0.13 eV (AB2 structure) to −0.28 eV (AA2 structure), to be compared with 0.39 eV for monolayer C_3N. These results suggest that interlayer chemical interactions have strong effects on the band edge states, resulting in a band gap reduction of as much as 0.67 eV. These results are expected since the band edge states are mostly derived from carbon p_z states (with some admixture of nitrogen p_z states) as shown in figure 2. These out-of-plane oriented states can be strongly affected by interlayer chemical interactions. For monolayer C_3N on substrates, the interfacial chemical coupling may also strongly modify its band edge states. In this case, however, the dielectric screening from the substrate will have additional effects and further renormalizes the quasiparticle band gap of C_3N, which will be discussed in the next section in the context of bulk phase C_3N.

Considering the relatively small overlap (0.17–0.28 eV) between the valence and conduction bands of the AA1 and AA2 structures calculated at the DFT level, all four bilayer structures are expected to be semiconductors when the GW quasiparticle corrections are included. We have carried out fully converged GW calculations for all bilayer structures. The convergence behavior of the calculated GW band gap for bilayer systems is similar to that shown in figures 3 and 4 for the monolayer, therefore we will not repeat here. There are subtle issues, however, that deserve mentioning. For the AA1 and AA2 structures, DFT predicts semimetallic band structures, which in turn give rise to (unphysical) metallic dielectric screening in the subsequent GW calculations if not treated properly. To restore the expected semiconductor dielectric properties, we apply a small scissors' shift (0.4 eV) to the DFT band structure so that a small band gap is opened up between valence and conduction bands. This scissors' shift is later taken out in the final GW results.

After including the quasiparticle corrections, all four bilayer structures are indeed semiconductors with band gaps ranging from 0.87 to 1.35 eV as shown in table 2. Interestingly, the quasiparticle correction to the band gap for the bilayer structures (ranging from 1.1 to 1.2 eV) is very similar to that for monolayer C_3N. The AB1 and AB2 stackings clearly have larger band gaps, presumably due to the fact that in these two structures only half of the atoms are directly on top of each other, thus reducing the interlayer chemical coupling effects.

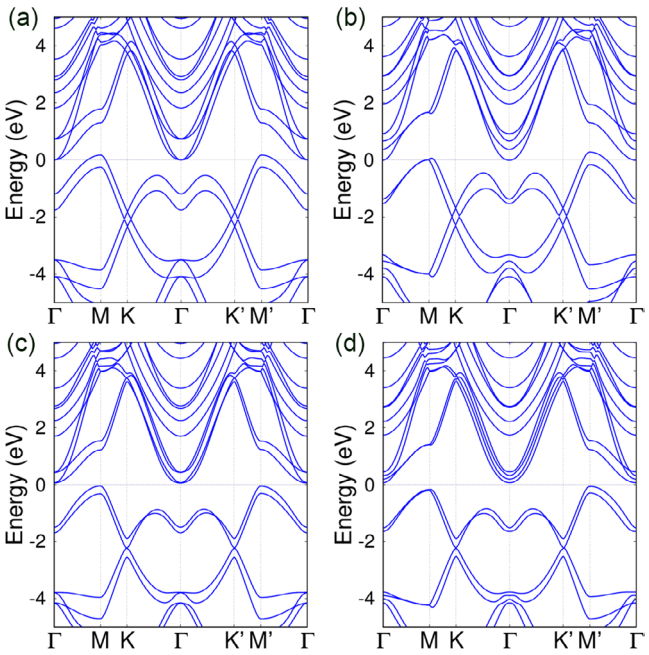

Figure 6. DFT-PBE band structures of four bilayer C_3N structures: (a) AA1, (b) AA2, (c) AB1, and (d) AB2. The interlayer interaction introduces bonding-antibonding splitting, resulting in a significantly reduced band gap compared with that of the monolayer system.

Table 2. Comparison between the DFT and GW band gaps of monolayer, bilayer, and bulk C_3N structures.

	Monolayer	Bilayer				Bulk			
		AA1	AA2	AB1	AB2	AA1	AA2	AB1	AB2
DFT	0.39	−0.17	−0.28	0.10	0.13	−0.98	−0.98	−0.14	−0.05
GW	1.50	1.07	0.87	1.34	1.35	—	—	0.56	0.60

Table 3. Optimized bulk structural parameters (*a* is the in-plane lattice constant and *d* is the inter-layer distance), and the relative energies (meV/atom) using different functional for the four different stacking models.

Functional	PBE			optB86b-vdW			SCAN+rVV10		
Stacking	*a* (Å)	*d* (Å)	Energy (meV)	*a* (Å)	*d* (Å)	Energy (meV)	*a* (Å)	*d* (Å)	Energy (meV)
AA1	4.860	3.833	1.6	4.858	3.323	10.3	4.828	3.291	10.1
AA2	4.860	3.722	0.0	4.857	3.187	0.0	4.828	3.179	0.0
AB1	4.861	3.762	0.5	4.859	3.237	3.4	4.830	3.194	1.0
AB2	4.861	3.744	0.5	4.860	3.225	2.3	4.830	3.196	0.1

Bulk C_3N

Dielectric screening effects on the quasiparticle properties of 3D bulk systems are fundamentally different from their 2D counterparts. In much the same way, when atomically thin 2D materials are placed on substrates, the screening effects from the substrate can also substantially renormalize the quasiparticle properties of the 2D overlayer, although the screening effects are reduced and come from only one side of the material. Here we investigate the electronic structure of bulk phase C_3N. This study, together with the results for monolayer and bilayer systems discussed earlier, will help to illustrate the interlayer chemical coupling and the bulk screening effects on the calculated quasiparticle band gap of C_3N.

We study four bulk stacking structures similar to those described in the previous section. The calculated structural parameters and relative energies are summarized in table 3. The PBE functional significantly overestimates the interlayer separations. Within the results calculated using vdW functionals, the AA1 stacking clearly has a higher energy, whereas the other three structures are essentially degenerate. The small energy differences indicate that these three stacking models may coexist in the as-synthesized samples. We will again use the structures optimized using the optB86b-vdW functional for subsequent electronic structure calculations.

Figure 7 shows the DFT-PBE band structures of the four bulk phases. Compared with the band structures

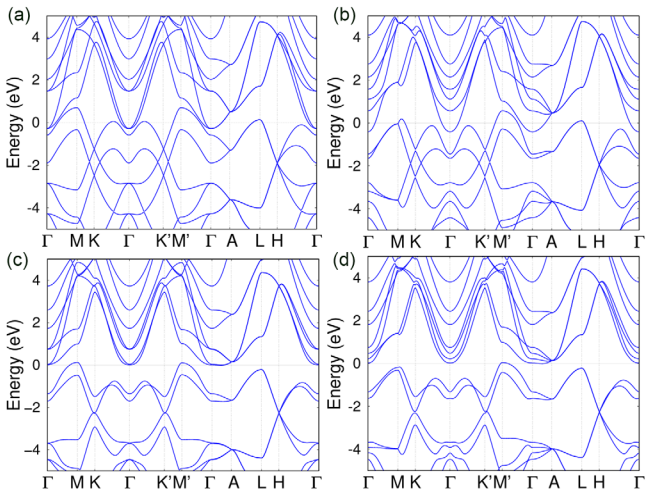

Figure 7. DFT-PBE band structures of four bulk C_3N structures: (a) AA1, (b) AA2, (c) AB1, and (d) AB2. The interlayer interaction introduces bonding-antibonding splitting, resulting in further reduced band gaps compared with those of the corresponding bilayer systems.

of the bilayer systems shown in figure 6, the interlayer coupling in the bulk phases introduces additional bonding-antibonding splittings and further reduces the DFT band gap. The interlayer coupling is so strong in the AA1 and AA2 structure that the valence and conduction bands severely overlap. The AB1 (AB2) structure, on the other hand, shows a small overlap of 0.14 eV (0.05 eV). Subsequent GW calculations suggest that the AA1 and AA2 structure remains metallic whereas the AB1 and AB2 structures are semiconductors with a small band gap of about 0.6 eV as summarized in table 2. The GW self-energy correction to the band gap of the AB1 (AB2) structure is 0.7 eV (0.65 eV). These values are significantly smaller than those for monolayer or bilayer systems.

Summary

We have systematically studied the electronic structures of monolayer, bilayer and bulk C_3N within the DFT and GW approaches. Our GW calculations unequivocally establish that the minimum quasiparticle band gap of monolayer C_3N is about 1.5 eV, an ideal value for electronics applications. Our result is in stark contrast with a recent experimental measurement [13], and we call for future experiments to verify our theoretical prediction. Interestingly, all four studied bilayer structures are nearly degenerate energetically, but the calculated band gap depends sensitively on the stacking pattern. Interlayer chemical coupling in the bilayer systems reduces the calculated quasiparticle band gap to 0.87–1.35 eV depending on the layer stacking. Unfortunately, we cannot make a firm prediction for the quasiparticle band gap of bulk phase C_3N. On one hand, different bulk stackings are nearly degenerate energetically. On the other hand, their electronic band structures are very sensitive to the interlayer chemical coupling, which in turn depends strongly on the stacking pattern. The calculated quasiparticle band structures of four bulk C_3N structures suggest that the bulk phase may be metallic or semiconducting depending on the layer stacking. Experimentally, various bulk phases may coexist in the as-synthesized samples unless kinetics somehow prefers or prohibits certain stacking patterns. This issue definitely deserves further investigations.

Acknowledgments

Work at SHU was supported by National Key Basic Research Program of China (Grant No. 2015CB921600), the National Natural Science Foundation of China (Grant No. 51672171 and No. 11628407), the fund of the State Key Laboratory of Solidification Processing in NWPU (SKLSP201703) and the Eastern Scholar Program from the Shanghai Municipal Education Commission. Special Program for Applied Research on Super Computation of the NSFC-Guangdong Joint Fund (the second phase), the supercomputing services from AMHPC, the Fok Ying Tung Education Foundation and the Center for Computational Research at UB are acknowledged. Work at UB was supported by the US-NSF under Grant No. DMR-1506669 and No. DMREF-1626967. Y W acknowledges the support from China Scholarship Council.

ORCID iDs

Yabei Wu https://orcid.org/0000-0002-6016-7115
Weiwei Gao https://orcid.org/0000-0003-4477-393X
Fanhao Jia https://orcid.org/0000-0002-9645-8395
Peihong Zhang https://orcid.org/0000-0002-0836-316X

References

[1] Zhou S Y, Gweon G-H, Fedorov A, First P, De Heer W, Lee D-H, Guinea F, Neto A C and Lanzara A 2007 Substrate-induced bandgap opening in epitaxial graphene *Nat. Mater.* **6** 770

[2] Giovannetti G, Khomyakov P A, Brocks G, Kelly P J and Van Den Brink J 2007 Substrate-induced band gap in graphene on hexagonal boron nitride: *ab initio* density functional calculations *Phys. Rev.* B **76** 073103

[3] Jung J, DaSilva A M, MacDonald A H and Adam S 2015 Origin of band gaps in graphene on hexagonal boron nitride *Nat. Commun.* **6** 6308

[4] Nevius M, Conrad M, Wang F, Celis A, Nair M, Taleb-Ibrahimi A, Tejeda A and Conrad E 2015 Semiconducting graphene from highly ordered substrate interactions *Phys. Rev. Lett.* **115** 136802

[5] Gebhardt J, Koch R, Zhao W, Höfert O, Gotterbarm K, Mammadov S, Papp C, Görling A, Steinrück H-P and Seyller T 2013 Growth and electronic structure of boron-doped graphene *Phys. Rev.* B **87** 155437

[6] Zhao L, He R, Rim K T, Schiros T, Kim K S, Zhou H, Gutiérrez C, Chockalingam S, Arguello C J and Pálová L 2011 Visualizing individual nitrogen dopants in monolayer graphene *Science* **333** 999

[7] Liu A Y and Cohen M L 1989 Prediction of new low compressibility solids *Science* **245** 841

[8] Wei W and Jacob T 2013 Strong excitonic effects in the optical properties of graphitic carbon nitrideg-C_3N_4 from first principles *Phys. Rev.* B **87** 085202

[9] Du A, Sanvito S and Smith S C 2012 First-principles prediction of metal-free magnetism and intrinsic half-metallicity in graphitic carbon nitride *Phys. Rev. Lett.* **108** 197207

[10] Cui P, Choi J H, Zeng C, Li Z, Yang J and Zhang Z 2017 A kinetic pathway toward high-density ordered N doping of epitaxial graphene on Cu(1 1 1) using C_5NCl_5 precursors *J. Am. Chem. Soc.* **139** 7196

[11] Xiang H J, Huang B, Li Z Y, Wei S H, Yang J L and Gong X G 2012 Ordered semiconducting nitrogen-graphene alloys *Phys. Rev.* X **2** 011003

[12] Wang Y, Lv J, Zhu L and Ma Y 2010 Crystal structure prediction via particle-swarm optimization *Phys. Rev.* B **82** 094116

[13] Yang S *et al* 2017 C_3N—A 2D crystalline, hole-free, tunable-narrow-bandgap semiconductor with ferromagnetic properties *Adv. Mater.* **29** 1605625

[14] Mahmood J *et al* 2016 Two-dimensional polyaniline (C_3N) from carbonized organic single crystals in solid state *Proc. Natl Acad. Sci. USA* **113** 7414

[15] Shi Z, Kutana A and Yakobson B I 2015 How much N-doping can graphene sustain? *J. Phys. Chem. Lett.* **6** 106

[16] Qiu D Y, da Jornada F H and Louie S G 2017 Environmental screening effects in 2D materials: renormalization of the bandgap, electronic structure, and optical spectra of few-layer black phosphorus *Nano Lett.* **17** 4706

[17] Hybertsen M S and Louie S G 1986 Electron correlation in semiconductors and insulators: band gaps and quasiparticle energies *Phys. Rev.* B **34** 5390

[18] Deslippe J, Samsonidze G, Strubbe D A, Jain M, Cohen M L and Louie S G 2012 BerkeleyGW: a massively parallel computer package for the calculation of the quasiparticle and optical properties of materials and nanostructures *Comput. Phys. Commun.* **183** 1269

[19] Kresse G and Hafner J 1993 *Ab initio* molecular dynamics for liquid metals *Phys. Rev.* B **47** 558

[20] Kresse G and Furthmuller J 1996 Efficiency of *ab initio* total energy calculations for metals and semiconductores using a plane-wave basis set *Comput. Mater. Sci.* **6** 15

[21] Perdew J P, Burke K and Ernzerhof M 1996 Generalized gradient approximation made simple *Phys. Rev. Lett.* **77** 3865

[22] Klimes J, Bowler D R and Michaelides A 2010 Chemical accuracy for the van der Waals density functional *J. Phys.: Condens. Matter* **22** 022201

[23] Sun J, Ruzsinszky A and Perdew J P 2015 Strongly constrained and appropriately normed semilocal density functional *Phys. Rev. Lett.* **115** 036402

[24] Monkhorst H J and Pack J D 1976 Special points for Brillouin-zone integrations *Phys. Rev.* B **13** 5188

[25] Gao W, Xia W, Gao X and Zhang P 2016 Speeding up GW calculations to meet the challenge of large scale quasiparticle predictions *Sci. Rep.* **6** 36849

[26] Ismail-Beigi S 2006 Truncation of periodic image interactions for confined systems *Phys. Rev.* B **73** 233103

[27] Wang H, Wu H and Yang J 2017 C_3N: a two dimensional semiconductor material with high stiffness, superior stability and bending Poisson's effect (arXiv:1703.08754)

[28] Hong Y, Zhang J and Zeng X C 2018 Monolayer and bilayer polyaniline C_3N: two-dimensional semiconductors with high thermal conductivity *Nanoscale* **10** 4301

[29] Gao W, Xia W, Wu Y, Ren W, Gao X and Zhang P 2018 Quasiparticle band structures of CuCl, CuBr, AgCl, and AgBr: the extreme case *Phys. Rev.* B **98** 045108

[30] Shih B C, Xue Y, Zhang P, Cohen M L and Louie S G 2010 Quasiparticle band gap of ZnO: high accuracy from the conventional $G(0)W(0)$ approach *Phys. Rev. Lett.* **105** 146401

[31] Felipe H, Qiu D Y and Louie S G 2017 Nonuniform sampling schemes of the Brillouin zone for many-electron perturbation-theory calculations in reduced dimensionality *Phys. Rev.* B **95** 035109

[32] Qiu D Y, Felipe H and Louie S G 2013 Optical spectrum of MoS_2: many-body effects and diversity of exciton states *Phys. Rev. Lett.* **111** 216805

[33] Rasmussen F A, Schmidt P S, Winther K T and Thygesen K S 2016 Efficient many-body calculations for two-dimensional materials using exact limits for the screened potential: band gaps of MoS_2, h-BN, and phosphorene *Phys. Rev.* B **94** 155406

[34] Hüser F, Olsen T and Thygesen K S 2013 How dielectric screening in two-dimensional crystals affects the convergence of excited-state calculations: monolayer MoS_2 *Phys. Rev.* B **88** 245309